Research Square

Preprints are preliminary reports that have not undergone peer review.
They should not be considered conclusive, used to inform clinical practice,
or referenced by the media as validated information.

Growth and Characterization of Structural Optical Elctrical and Nonlinear Optical Studies of Piperazine Sulphanate Single Crystal

K. Mahalakshmi
Presidency College
J. Shalini
Presidency College
P. Surendran
Arignar Anna Government Arts College
S. Periyasamy
Presidency College
B. Sahaya Infant Lasalle
Sri Sivasubramaniya Nadar College of Engineering
Muthu Senthil Pandian
Sri Sivasubramaniya Nadar College of Engineering
P Rameshkumar
rameshkumarevr@gmail.com
Presidency College
Karthik Kannan
Karpagam Academy of Higher Education

Research Article

Keywords: Crystal growth, Structural, optical, electrical properties, and NLO

Posted Date: October 30th, 2026

DOI: https://doi.org/10.21203/rs.3.rs-11384641/v1

License: This work is licensed under a Creative Commons Attribution 4.0 International License.
Read Full License

Additional Declarations: No competing interests reported.

GROWTH AND CHARACTERIZATION OF STRUCTURAL OPTICAL ELCTRICAL AND NONLINEAR OPTICAL STUDIES OF PIPERAZINE SULPHANATE SINGLE CRYSTAL

K. Mahalakshmi[1], J. Shalini[1], P. Surendran[2], S. Periyasamy[1], B. Sahaya Infant Lasalle[3], Muthu Senthil Pandian[3], P. Rameshkumar[1,*] Karthik Kannan[4]

[1]PG and Research Department of Physics, Presidency College, Chennai, Tamil Nadu 600 005, India

[2]PG and Research Department of Physics, Arignar Anna Government Arts College, Namakkal, Tamil Nadu, 637 002, India

[3]SSN Research Centre, Sri Sivasubramaniya Nadar College of Engineering, Chennai, Tamil Nadu 603 110, India

[4]Department of Physics, Center for Energy and Environment, Karpagam Academy of Higher Education, Coimbatore, Tamil Nadu 641021, India

---

***Corresponding author**

E-mail address: rameshkumarevr@gmail.com (Dr. P. Rameshkumar)

ABSTRACT

Single crystal of piperazine sulphanate (PSA) was grown using slow evaporation method by adding solvent as methanol at room temperature. The PSA crystalline material was confirmed structurally by the study of Single crystal x- ray diffraction studies (SCRD) as it shows that the crystal grown was orthorhombic in crystal structure and belong to space group of Pbca. Different functional groups presents was revealed by FT-IR spectroscopy. From the studies of UV-Vis absorption spectrum, the value of lower cut- off wavelength is found as 350 nm and its energy band gap and extinction coefficient has been calculated. Dielectric properties of grown crystal was investigated for dielectric constant and dielectric loss and further, the calculation for the electronic polarizability of the grown crystal was done using Penn analysis and Clausius-Mossotti equation and that are in good agreement. The Photoconductivity measurements of the sample reveals that the PSA crystal has negative

photoconductive nature. Intermolecular interactions of PSA has been tested through Hirshfeld surface analysis. It reveals that H…H are the higher interactions (36.2%) in the Hirshfeld surface of the molecule. The Z-Scan analysis is used to find the third order non-linear susceptibility of the crystal using He-Ne laser as the source of wavelength 632.8nm.

Keywords

Crystal growth, Structural, optical, electrical properties, and NLO

---

1. Introduction

Since 1980s, research on nonlinear optical (NLO) materials has progressed rapidly, fueled by the increasing demand for materials exhibiting strong optical nonlinearity for various commercial applications, including optical limiters, data storage devices, photonic technologies, and advanced signal-processing systems [1–3]. Over the past few years, researchers have increasingly focused on integrating nonlinear optical (NLO) crystals into laser and sensor technologies [4,5]. The growth of the third order nonlinear optically transparent organic single crystals has gained prominence because of their remarkable nonlinear optical efficiency and high optical damage threshold, comparable with conventional inorganic materials [6]. Organic nonlinear materials exhibit significant and ultrafast third-order frequency conversion capabilities, along with tunable molecular properties enabled by molecular engineering and advanced synthetic methodologies and Organic single crystals are primarily stabilized by weak van der Waals interactions, extended π-conjugated electron systems, and hydrogen-bond networks. These structural features facilitate effective intermolecular charge transfer, which significantly enhances nonlinear electro-optical properties. From an application perspective, organic crystals exhibiting strong nonlinear responses and superior crystalline quality are highly desirable for advanced photonic and optoelectronic devices[7,8,9] The enhanced nonlinear optical efficiency of a sample is primarily attributed to strong hydrogen-bonding interactions. Organic NLO materials have attracted considerable interest in photonics and laser technology due to their remarkable properties, including photochromism, two-photon absorption, luminescence, ultrafast response times, favorable wavelength dispersion characteristics low refractive index[10]. The heterocyclic compound piperazine atom has six-membered ring having two nitrogen atoms

placed opposite to each other within the ring framework. Owing to its strong hydrogen-bonding capability, piperazine readily forms supramolecular assemblies. Its diamine functionality and cyclic structure make it particularly effective as an agent for CO_2 capture and recovery. In addition, piperazine derivatives serve as important constituents in certain anthelmintic drugs provide inhibit to the growth and multiplication of intestinal parasites in the body of pets and livestock. Furthermore, because of material property to coordinate with the metal ions, piperazine-based compounds are widely employed as chelating agent [11]. Sulphanilic acid adopts a zwitterionic configuration in the solid state, and the molecules are connected robust three-dimensional supramolecular network via two different types of two-central bonds that are N–H···O hydrogen bonds and presence of the planar three-centre N–H···$(O)_2$ hydrogen bond[12]. The presence of zwitterionic groups and the adaptable chemical nature of sulphanilic acid make it a promising material for manipulating optical signal efficiency through targeted structural modifications. Recently piperazine crystal such as Piperazinium ammonium chloride hydrate, piperazinium bis (trifluoroacetate) ,piperazinium-2-nitrobenzoate, Piperazinium citrate, Piperazinum Isophthalate was reported [13–17]. Sulphanilic acid was reported as Sulfanilic Acid Single Crystal, Guanidinium Sulphanilate, diisopropylammonium 4-aminobenzenesulfonate, Piperazine-1, 4-diiumbis (4-aminobenzenesulfonate) [18–21]. The crystal structures of Piperazine sulphanate was already studied by P. Rekha et al. [22]**.**

In this present work, Some important characterization were analyzed and details of PSA crystal has been explained for the first time through this communication. PSA single crystal has been grown by method of slow solvent evaporation method. The grown crystal was tested for XRD, UV, FTIR Dielectrics, Photoconductivity, Hirshfield surface analysis and Z-Scan.

2. Synthesis and Crystal growth

Piperazine sulphanate (PSA) single crystals was harvested by the slow evaporation solution growth method by the use of solvent as methanol. Analytical reagent (AR) grade piperazine and sulphanilic acid were used without further purification. Equimolar (1 M) solutions of piperazine and sulphanilic acid were prepared separately by dissolving the required quantities in methanol. The two solutions was then poured together and stirred continuously for 6 h to obtain a clear and homogeneous solution, ensuring complete reaction between the starting materials. The resulting solution has been filtered to remove any insoluble impurities and

obtain a clear solution suitable for crystal growth. The filtered solution was transferred into a clean crystallization vessel and kept undisturbed at room temperature in a dust-free atmosphere to allow slow evaporation of the solvent. As the solvent gradually evaporated, nucleation occurred, followed by the growth of well-defined single crystals. After a growth span of 25 days, clear, transparent and optically good-quality single crystals piperazine sulphanate (PSA) was successfully grown. The photograph of harvested PSA single crystal was given in the Figure 1.

3. Characterization studies

The Unit cell structural parameters of the grown crystal PSA were confirmed by SCXRD using X8 Kappa APEXII (Bruker) using monochromatic MoK_α radiation as source (λ= 0.717 Å) In PXRD was measured using (PANalytical Empyrean) CuK_α radiation as the source k = 1.5406 Å to find various diffraction planes of the grown crystal. Vibrational analysis was characteristics by using FTIR (Bruker AXS FTIR Spectrometer) Shimadzu, UV- 2600 spectrometer has been used to find the transmittance of PSA single crystal. Bruker AXS FTIR spectrometer has been used to analyze the vibrational modes. In frequency range of 1Hz to 1MHz the dielectric properties of PSA was investigated using PSM 1735 LCR. Keithley picoammeter of the Model M6487 has been used to find the photoconductivity. Hirshfeld surface analysis for studying the interaction between the molecules are done through software Crystal Explorer 07 and the nonlinearity of order three were studied using Z-Scan method while passing the continuous wave (CW) of He-Ne laser (21mW) of wavelength 632.8nm as source.

4. Results and Discussion

4.1 X-Ray Diffraction (XRD)

The Single crystal XRD gives the structural conformation details confirmed of PSA crystal and the structural parameters of PSA grown crystal are found as a = 10.21291 Å, b = 8.50465 Å, c = 21.64040 Å α=90° β=90.46° γ= 90° and V= 1873.2 $Å^3$ with orthorhombic crystal system belongs to Pbca space group, Which are of with the good agreement with already reported values of PSA crystal [22]. Powder X-ray Diffraction (PXRD) is a unique technique that use X-rays to investigate the crystallographic and molecular structures of the substance. The specimen undergoing analysis is meticulously ground into fine powder and homogenized after which its average bulk composition is accurately determined. The respective indexed PXRD pattern is shown in the Figure 2(a).

Using Hall- Willamson equation, the strain value present in the lattice of grown PSA crystal has been calculated using the formula

$$\beta cos\theta = \frac{k\lambda}{D} + 4\eta \mathrm{Sin}\theta \quad (1)$$

Where β refers to full width half maximum values of the diffraction peaks, θ refers to the angle of the diffraction, K refers to the Scherrer constant, λ refers to the wavelength of used X-ray and D refers to crystallite size. A graph is drawn between $\beta cos\theta$ and 4Sinθ as shown in the Figure 2 (b).

The estimated strain value of the PSA crystal is 0.00153. The positive value of slope proposes that the obtained strain is compressive and the impurities are incorporated into the lattice's interstitial positions [24].

3.2 FTIR Analysis

Infrared spectroscopy examines the vibrational and rotational behavior of molecules. When exposed to infrared radiation, molecules absorb energy at characteristic wavelengths, enabling the identification of their molecular structure and functional groups. Fourier Transform Infrared (FTIR) technique is an essential technique that is used to determine the various functional groups and investigate chemical bond interactions within a material. FTIR spectrum of the grown crystal PSA crystal was given in the Figure 3. The broad band of absorption centered at 3384 cm^{-1} is corresponding with N–H stretching vibration of the protonated piperazine and the absorption bands found at 3129 cm^{-1} and 3033 cm^{-1} are belong to aromatic C–H stretching of the sulphanilic acid ring. The prominent peaks at 1287 cm^{-1} and 1238 cm^{-1} are attributed to C–N stretching of the piperazine ring along with contributions from S–O stretching vibrations of the sulfonate group. The absorption bands located at 1142 cm^{-1} and 1026 cm^{-1} are the characteristic of asymmetric and symmetric stretching vibrations of SO_3^- group, which confirming the presence of the sulphanilic acid moiety in the crystal. The bands observed at 878 cm^{-1}, 816 cm^{-1}, and 754 cm^{-1} are belongs to aromatic C–H out-of-plane bending vibrations, while the peaks that are at 713 cm^{-1} and 554 cm^{-1} are associated with C–S stretching and deformation vibrations of the aromatic sulfonate group.

3.3 UV-Visible Analysis

UV Visible analysis is one of the effective technique to characterize materials through studying the way that material interact with the light. It provides vital details about the

chemical composition, physical properties, optical characteristics, and electronic structure of a material. One of the most important properties of nonlinear optical crystal is to have good optical transmittance and for optical limiting devices fabrication optical transparency is necessary [25]. The UV-Vis spectrum explains the information of UV light and visible light which involves in the transmission of electron that are present in σ and π orbitals from the groundstates i.e. with the less energy level to the excited energy states of higher energy level [26]. The optical absorption spectrum was given in the Figure 4(a). It shows the optical edge at 350nm which was in the agreement with the already reported values. With help of the standard equation the optical band gap can be calculated,

$$(\alpha h\upsilon) = A(h\upsilon - E_g)^n \quad (2)$$

In above equation α represents the absorption coefficient, $h\upsilon$ represents the energy of photon, A represents the transition parameters (free from photon energy), n is equal to ½ for directly allowed and n is 2 for indirectly allowed transition. The tauc's plot for $(\alpha h\upsilon)^2$ versus energy of photon is shown in the Figure4(b). The band gap value of the grown crystal is 3.4 eV. The lower cut-off wavelength in visible region confirms the PSA crystal is suitable of optoelectronic applications [27].

The extinction coefficient (k) represents the absorption of electromagnetic radiation by the material. A lower value of (k) indicates reduced optical absorption and higher optical transparency are by using formula,

$$k = \frac{\alpha\lambda}{4\pi} \quad (3)$$

The extinction co-efficient versus wavelength graph is shown in the Figure 4(c). The optical analysis shows the grown PSA crystal exhibits excellent optical properties, making it a promising suitable candidate for optoelectronic device applications.

3.4 Dielectric Analysis

The dielectric analysis of grown PSA proves the information about the electric properties of crystal that decides the suitability for practical device application of the grown crystal. The PSA crystal cut and polished to measure the dielectric behaviour. The sample is both side coated with silver paste to make the electric contacts to reduce the air gap between the electrodes and to reduce the external polarization due to the air molecules. The parallel plate capacitor was formed by keeping materials in between the two copper electrode in the

center. The reading was taken in the rage of 1 Hz to 1MHz. The dielectric constant of grown crystal is measured at the room temperature has been calculated using the formula

$$\varepsilon_r = \frac{Cd}{\varepsilon_0 A} \quad (4)$$

Where C refers to the capacitance, d refers to the thickness of the material, A refers to the area of the material, and ε_0 refers to the permittivity of the free space (8.854×10^{-12} F/m).

The dielectric constant and dielectric loss graph was shown in the Figure 5(a) and 6(b). These figures suggest that Dielectric constant value decreases when the frequency value increases. Which indicates the presence of electronic, ionic, space charge and orientational polarization may result in the a high dielectric constant at the lower frequency level because of the dipoles are aligned to the specific directions.

And also dielectric loss is low at high frequency is due to presence or absence of above polarization effect using log f and tan δ graph[28]. The low loss value indicates the grown PSA crystals are of good quality and have fewer defects or impurities. Additionally the AC conductivity measurement was performed using the relation

$$\sigma_{ac} = 2\pi f \varepsilon_r \varepsilon_0 tan\delta \quad (5)$$

Where ε_0 refers to permittivity of free space and f refers to applied frequency (Hz) $tan\delta$ is the dielectric loss [29]. The deviation of the AC conductivity values with the corresponding applied frequency is depicted in the Figure 7.

3.5 Determination of solid state parameters

The electronic polarizability values of the grown crystal is based on the number of valence electron, Penn gap, plasma energy, Fermi energy and electronic polarizability was theoretically calculated. From experimental values of the dielectric analysis, it is revealed that the because of the valence electron, Penn gap, Fermi energy, and electronic polarizability, dielectric constant is high. The density was calculated using

$$\rho = \frac{MZ}{N_A V} \quad (6)$$

Where M refers to molecular weight of PSA, Z refers to the molecular unit cell, V refers to volume of unit cell and N_A represents Avogadro number. The value of valence electron plasma energy was calculated using,

$$\hbar\omega_\rho = 28.8\sqrt{\frac{(Z \times \rho)}{M}} \quad (7)$$

The sum of all valence electron presents in the PSA crystal is Z= (16*4) + (24*1) + (4*5) + (6*6) + (2*6) = 156 here, ρ refers to density and the number of valence electron present in C, H, N, O and S atoms are 4, 1, 5, 6, 6.

The average Penn gap calculated using the formula,

$$E_P = \frac{\hbar\omega_\rho}{\sqrt{\varepsilon_r - 1}} \quad (8)$$

The fermi energy value was calculated by using the formula,

$$E_F = 0.2948(\hbar\omega_\rho)^{4/3} \quad (9)$$

Electronic polarizability can be calculated using,

$$\alpha = \frac{(\hbar\omega_\rho)^2 S_0}{(\hbar\omega_\rho)^2 S_o + 3E_p^2} \times \frac{M}{\rho} \times 0.369 \times 10^{-24}\, cm^3 \quad (10)$$

Where $S_O = 1 - \frac{E_p}{4E_F} + \frac{1}{3} + [\frac{E_p}{4E_F}]^2$

By using Clausius- Mosotti relation the electronic polarizability (α) is calculated using,

$$\alpha = \frac{3M}{4\pi N_A \rho}\left(\frac{\varepsilon' - 1}{\varepsilon' + 2}\right) \quad (11)$$

ε' refers to the dielectric constant of the material at the room temperature. The calculated solid state parameters values of PSA crystal was tabulated in the Table 1. All crystal with good solid state parameters, lesser defect along with calculated parameters is important properties for NLO applications.

3.6 Photoconductivity

Photoconductivity is the method by which a crystal's electrical conductivity improves upon absorbing the electromagnetic radiation. It refers to the change in a crystal's electrical conductivity (σ) due to radiation exposure. Photoconductivity increase with the electrical conductivity of a crystal that happens when the crystal is subjected to infrared, visible or ultraviolet light [30]. Initially, to connect the copper electrodes and samples, silver paint is

applied on the top of the grown crystal, after that they are placed in the vacuum. By supplying the direct current voltages of value from 0 to 50V of increments of 1 V/s, without the radiation the dark current was measured. Followed by radiation of 50W halogen light exposed to the sample the photocurrent was recorded over the supplied voltage range of 0 to 50V with the increments of 1V/s. The Photoconductivity plot of the PSA crystal is given in the Figure 6. The plots of the photocurrent and dark current depends on applied voltage shows the dark current was consistently greater than the photo current. This indicates that grown crystal PSA exhibits the negative photoconductivity nature is because there is the reduction in the amount of charge carriers on their time of applied radiation. Again under the presence of radiation the combines the electrons and holes occurs that results in the reduction in total number of the mobile charge carriers present in conduction band in the existence of radiations resulting in negative photoconductivity [31,32]. The photosensitivity of the material is calculated as 0.00949 by using the relation,

$$\text{Photosensitivity} = \frac{I_p - I_d}{I_d} \tag{12}$$

Where, I_p represents photocurrent and I_d represents dark current. The Negative photoconductive material, due to their unique ability allows them to respond effectively to infrared radiation and ultraviolet radiation, making the grown crystal suitable components in sensing and detection device applications. [33,34].

3.7 Hirshfeld Surface Analyses

Hirshfeld surface analysis give the deep knowledge about the intermolecular interactions of the crystal state by using the electron density present with the molecular contact points. The 3D Hirshfeld and two dimensional fingerprint plots are not only used for the purposes of visualization of intermolecular interactions which stabilize the crystal structure but also provide valuable information for the contributor interaction to the surface[35,36]. The Crystal Explorer 17.5 software was the key tool used to calculate the Hirshfeld surface and their corresponding fingerprint plots using the crystallographic information data (CIF). The 3 D plots are shown in the Figure 7**.** In the d_{norm} blue and white surface is higher than the red surface in the complex is due to hydrophobic area. Whereas the dark red and blue coloured surfaces of the shaped index represents the C-H…π interaction on the crystal. The input intermolecular interactions to the crystal surface was evaluated using 2D finger print plots and the intermolecular contacts contributions are given in the Table 2.

3.8 Z Scan Analysis

The Z-scan analysis is a accurate, and are highly very sensitive in the use of single-beam method extensively used to characterize nonlinearity of third order optical behavior of the samples. The measurement are performed by moving the crystal along the z-axis direction through the focus point of the Gaussian laser beam and recording the far-field transmittance, that is given out is depends on the position of the sample. The experimental data obtained from this technique provide valuable information about the nonlinear absorption coefficient of material and the nonlinear refractive index of the sample. Materials possessing enhanced nonlinear optical characteristics are considered promising candidates for the fabrication of ultrafast optical switches, optical modulators, optical communication systems, laser protection devices, and various photonic and optoelectronic applications [37]. The value of nonlinear refractive index (n_2) were determined from results of the closed-aperture of Z-scan measurements where intensity of the sample is measured by keeping an aperture in between the lens and the detector. and whereas the magnitude of nonlinear absorption coefficient (β) value was evaluated using results of open-aperture value of Z-scan measurements where the intensity is recorded by the placing the lens in the front of detector. The combined analysis of closed-aperture and open-aperture of Z-scan results provides a reliable and comprehensive assessment of the third-order nonlinear optical characteristics of the sample [38]. The Z-Scan work in the principle that in the illumination of high intensity laser beam radiation, and the process of absorption and refraction depends on the intensity of laser beam which is used as source. The property of nonlinear optical property of PSA crystal has been investigated with the help of the Z-scan analysis with the use of He–Ne laser with the wavelength of 632.8 nm. The PSA crystal was moved through the focal points of a Gaussian laser beam with the help of a digitally controlled stepper motor, while the transmitted laser intensity was measured with a photodetector. The material was scanned towards the z-axis direction from negative value of −Z to positive value of +Z direction through the focus of a 300 mm focal-length lens. The nonlinear optical characteristic of PSA crystal were measured using the Z-scan analysis under both open aperture (OA) and closed aperture (CA) configurations. The open aperture Z-scan curve exhibits a symmetric transmission profile around the focal position, indicating the nonlinear absorption property of the material. The observed variation in transmission close to the focus confirms that the incident laser intensity induces intensity-dependent absorption, demonstrating the nonlinear optical response of the crystal. The OA behavior suggests that the material possesses

significant nonlinear absorption characteristics, which are beneficial for optical limiting and laser protection applications.

The CA Z-scan measurement shows a distinct peak–valley transmission pattern around the focal point, confirming the existence of nonlinear refraction in the PSA crystal. This characteristic transmittance profile arises from the laser-induced change in the refractive index of the crystal under high optical intensity. The observed nonlinear refraction indicates that the crystal exhibits an appreciable third-order nonlinear optical property[39]. Figure 9(a) & (b) shows the open aperture and closed aperture curve of the sample. The combination of nonlinear absorption and nonlinear refraction demonstrates that PSA crystal is promising third-order optical nonlinearity, that are suitable for photonic and optoelectronic applications like optical switching, optical modulation, optical limiting, and nonlinear signal processing.

Nonlinear absorption coefficient (β) has been found as follows

$$n_2 = \frac{\Delta\phi}{KI_O Le_{ff}} \tag{13}$$

Where $\Delta\boldsymbol{\phi}$, K represent phase shift and wave number, L_{eff} represents to the effective thickness of the crystal.

Nonlinear absorption coefficient (β) has been found as follows

$$\beta = \frac{2\sqrt{2}\Delta T}{I_O Le_{ff}} \text{(m/w)} \tag{14}$$

The real and imaginary part of the nonlinearity of order three susceptibility is calculated using

$$\text{Re}\chi^{(3)} = \frac{10^{-4}\varepsilon_o c^2 {n_o}^2 n_2}{\pi} \text{(cm}^2\text{/W)} \tag{15}$$

$$\text{Im}\chi^{(3)} = \frac{10^{-2}\varepsilon_o c^2 {n_o}^2 \lambda\beta}{4\pi^2} \text{(cm/W)} \tag{16}$$

Where ε_o represents the vacuum permittivity is 8.854 x 10^{-12} F/m, c represents velocity of light in free space and here, n_o represents the linear refractive index of the material.

NLO susceptibility is calculated as follows.

$$\chi^{(3)} = \sqrt{(R_e\chi^{(3)})^2 + (I_m\chi^{(3)})^2} \quad \text{(cm/W)} \tag{17}$$

The value of third- order nonlinear susceptibility $\chi^{(3)}$ of the PSA crystal has been found to be 7.630976 x 10^{-7}(esu).

5. Conclusion

The organic transparent PSA crystal has been successfully grown using the slow evaporation solution growth method by the use of the solvent as methanol, over growth span of 25 days. The fundamental crystal structure was confirmed by single-crystal X-ray diffraction (SCXRD), while the good crystalline quality of grown crystal has been determined by powder X-ray diffraction (PXRD). The FTIR spectrum verified was the vibrational functional groups present in grown crystal. Using UV–Visible spectral measurements it is clear that the lower cut-off wavelength is of 350 nm and an optical band gap is of 3.4 eV, indicating good optical transparency. The dielectric studies confirms the electrical behaviour of the grown crystal, and the fundamental electronic polarizability parameters has been evaluated using Penn analysis and Clausius–Mossotti equation. Photoconductivity measurements demonstrated that the crystal exhibits negative photoconductive behaviour. The intermolecular interactions present within the PSA crystal were investigated using Hirshfeld surface analysis. Furthermore, the Z-scan analysis confirmed the nonlinear optical response of the grown crystal, indicating that the grown PSA crystal is suitable material for photonic and optoelectronic applications.

Authors contributions

K. Mahalakshmi: Conceptualization, Data curation, Formal analysis, Project administration. J. Shalini: validation and formal analysis. P. Surendran: Investigation, Methodology, Writing-review, editing and Software. S. Periyasamy: Formal analysis, Writing-review & editing. B. Sahaya Infant Lasalle- Supervision, Formal analysis. Muthu Senthil Pandian: Writing- review & editing, P. Rameshkumar: Supervision, Data curation, Methodology. Karthik Kannan: resource, software, and writing.

Data availability

No data was used for the research described in the article

Declaration of competing interest

The authors declare that they have no known financial interest or personal relationships that have appeared to influence the work reported in this paper.

Acknowledgement

One of the authors, Dr. B. Sahaya Infant Lasalle, Sri Sivasubramaniya Nadar College of Engineering, thanks SSN management for providing a postdoctoral fellow.

References

[1] Petkovic M, Vieira L and Dropka N 2025 Machine learning in crystal growth: A review of methods, data, and applications Progress in Crystal Growth and Characterization of Materials **71** 100689. https://doi.org/10.1016/j.pcrysgrow.2025.100689.

[2] Luigi Di Lauro, Stefania Sciara, Bennet Fischer, Junliang Dong, Optimization methods for integrated and programmable photonics in next-generation classical and quantum smart communication and signal processing systems Advances in Optics and Photonics **17** 526-622. https://doi.org/10.1145/3774905.3794680.

[3] Muthu K and Meenakshisundaram S 2012 Crystal growth, structure and characterization of p-Toluidinium picrate Journal of Crystal Growth **352** 163–6. https://doi.org/10.1016/j.jcrysgro.2011.11.058.

[4] Mourya V, Yadav S, Lohia P, Mishra A C, Dwivedi D K and Kulshrestha U 2025 High-precision alcohol sensing using twin core photonic crystal fiber Photonics and Nanostructures - Fundamentals and Applications **63** 101348. https://doi.org/10.1016/j.photonics.2024.101348.

[5] Yao Y, Chen Q, Li B, Zhang J, Wang R, Bai M, Liang R, Ma L, Ma T, Zhang J, Xia J, Nie H and Zhang B 2025 Influence of crystal orientation and incident plane on n-type 4H-SiC wafer slicing by using picosecond laser Optics & Laser Technology **182** 112174. https://doi.org/10.1016/j.optlastec.2024.112174.

[6] Lasalle B S I, Muthu S P, P. Karuppasamy, B.Gunasekaran and P. Ramasamy 2023 Synthesis, crystal growth and characterization of organic 1,2,4-triazole p-nitrophthalic acid (TPNP) single crystal for nonlinear optical (NLO) applications Inorganic Chemistry Communications **158** 111549. https://doi.org/10.1016/j.inoche.2023.111549.

[7] Thirumurugan R, Priyadharshini S, Babu B, Babu B M and Anitha K 2025 An efficient phase matching second harmonic generation of 2-amino-4-methylpyridinium quinoline-2-carboxylate (C16H15N3O2) organic single crystal: Structural, optical, thermal, and computational investigations Journal of Molecular Structure **1332** 141453. https://doi.org/10.1016/j.molstruc.2025.141453.

[8] Sudhakar G and Babu D R 2024 Synthesis and characterization of piperazine nitrate monochloride semi-organic single crystal for NLO applications Discov Appl Sci **6** 645. https://doi.org /10.1007/s42452-024-06341-y.

[9] Lasalle B S I, Muthu S P, Anitha K and Ramasamy P 2023 Synthesis, crystal growth and characterization of piperazinium 5-nitrosalicylate (P5NS) single crystal for nonlinear optical (NLO) applications Journal of Molecular Structure **1286** 135650. https://doi.org/10.1016/j.molstruc.2023.135650

[10] Purusothaman R, Shankar M, Dennis Raj A, Vimalan M and Vetha Potheher I 2023 A study on NLO, ultraviolet transparency, photoconductivity, and dielectric response of organic single crystal J Mater Sci: Mater Electron **34** 2292. https://doi.org/10.1007/s10854-023-11691-1.

[11] Lasalle B S I, Pandian M S, Anitha K and Ramasamy P 2023 Crystal growth and characterization of piperazinium mercuric chloride (PMC) single crystal for nonlinear optical (NLO) application Inorganic Chemistry Communications **157** 111397. https://doi.org/10.1016/j.inoche.2023.111397.

[12] Mythili P, Kanagasekaran T and Gopalakrishnan R 2007 Investigations on nucleation kinetics, growth and characterization of sulphanilic acid single crystals Cryst. Res. Technol. **42** 791–9. https://doi.org/10.1002/crat.200710907.

[13] Sivaraj R D, Gnanavel K, Kanchipuram Chandrasekar D S, Rajappan M J, Panneer selvam R and Gunasekaran R 2024 Crystal growth, structural, optical, laser damage threshold and nonlinear optical properties of Piperazinium citrate single crystal J Opt **53** 3198–206. https://doi.org/10.1007/s12596-023-01497.

[14] Priscilla J, Vijayaraghavan G V, Era P and Lakshmipriya M 2023 Crystal design of novel Piperazinum Isophthalate (PIP): Growth, Structural, Thermal, Spectral, Mechanical and Optical properties for NLO application Journal of Molecular Structure **1293** 136307. https://doi.org/10.1016/j.molstruc.2023.136307.

[15] Sivaraj S, Chidambaranathan B, Vijayamathubalan P, Gunaseelan R, Karuppasamy P, Sagayaraj P and Selvakumar S 2025 Piperazinium ammonium chloride hydrate: growth and physicochemical characterizations of nonlinear optical single crystal Journal of Molecular Structure **1337** 142117. https://doi.org/10.1016/j.molstruc.2025.142117.

[16] Sahaya Infant Lasalle B, Pandian M S, Anitha K and Ramasamy P 2025 Development and characterization of a novel organic piperazinium-2-nitrobenzoate single crystal for optoelectronic applications Optical Materials **167** 117369. https://doi.org/10.1016/j.optmat.2025.117369.

[17] Journal E B P, Sreedevi R, Sinthiya A S I J, Durai S C V, Balu T and Murugakoothan P 2024 Structural, Growth and Optical Characterization of Guanidinium Sulphanilate (GSA) Single Crystal Physics and Chemistry of Solid State **25** 278–83. https://doi.org/10.15330/pcss.25.2.278-283.

[18] Punithavathi, Thirupathy & Revathi 2024 An Investigation on Optical, Larvacidal and Cytotoxicity Analysis of Sulfanilic Acid Single Crystal for Optical and Biomedical Applications | Cell Biochemistry and Biophysics **83** 1139–1149. . https://doi.org/10.1007/s12013-024-01547-8.

[19] Saranya K, Muhildharani E and Raja C R 2023 Growth, structural confirmation and the effect of hydrogen bond on the third-order nonlinear optical properties of

diisopropylammonium 4-aminobenzenesulfonate crystal J Mater Sci: Mater Electron **34** 661. https://doi.org/10.1007/s10854-023-10088-4.

[20] Sathesh Kumar K, Prakash S M, Srinivasan P and Jayaprakash P 2024 Spectral studies and nonlinear optical properties of an organic crystal: Piperazine-1, 4-diiumbis (4-aminobenzenesulfonate) J. Nonlinear Optic. Phys. Mat. **33** 2350055. https://doi.org/10.1142/S0218863523500558.

[21] Rekha, Peramaiyan, NizamMohideen, Mohan Kumar and Et. A 2016 Synthesis, growth and characterization of a new organic three dimensional framework: Piperazin-1-ium 4-aminobenzenesulfonate Journal of Crystal Growth **441** 18-25. https://doi.org/10.1016/j.jcrysgro.2016.02.005.

[22] Jahil S S, Mohammed I A, Khazaal A R, Jasim K A and Harbbi K H 2022 Application the Halder–Wagner to calculation crystal size and micro NeuroQuantology **20** strain by X-ray diffraction peaks analysis 199–204. https://doi.org/10.14704/nq.2022.20.1.NQ22074.

[23] Mohanraj M and Parthasarathy M 2025 A comprehensive evaluation of nonlinear optical materials: Synthesis, growth, spectral, photoluminescence, LDT, photoconductivity, thermal, antibacterial and second harmonic generation analysis Solid State Communications **404** 116113. https://doi.org/10.1016/j.ssc.2025.116113.

[24] Sankaran Nampoothiri V, Varghese M, Sunil Raj R, Chandran S, Gummagol N and Joseph L 2025 Comprehensive Analysis of 4-Methoxybenzylammonium Nitrate (4MBAN): Synthesis, Spectroscopic (UV-vis, PL), Quantum Computation and Topological (ELF, LOL, RDG and AIM) Analysis Journal of Physics: Conference Series vol **3038** (IOP Publishing) p 012012

[25] Sahaya Infant Lasalle B, Muthu S P, Alexandar A, Narmadha S, Jeeva Govind R, Kumar M and Chang J-H 2025 Growth and functional characterization of piperazinium bis(sulfamate) single crystals for nonlinear optical and optoelectronic applications Solid State Communications **405** 116173. https://doi.org/10.1016/j.ssc.2025.116173.

[26] Dinagaran S, Gajendiran J, Raj S G and Gnanam S 2022 Study of crystalline growth, structural characteristics, optical behavior, thermo and dielectric properties of isoniazid single crystal Optics & Laser Technology **156.** https://doi.org/108576. 10.1016/j.optlastec.2022.108576

[27] Fawad M, Maqsood N, Nawaz A, Islam B, Zaheer M D and Skotnicová K 2025 Synthesis, Characterization, and Enhanced Optical and Dielectric Properties of Pure and Ni-Doped ZnO Nanoparticles for Advanced Electronic Applications Results in Engineering **26** 104824. https://doi.org/10.1016/j.rineng.2025.104824.

[28] Lasalle B S I, Pandian M S, Ramasamy P and Anitha K 2025 Crystal growth and characterization of a novel organic triethylenediaminium hydronium trinitrate (TEDHT) single crystal for optoelectronic applications J Mater Sci: Mater Electron **36** 188. https://doi.org/10.1007/s10854-025-14236-w.

[30] Vediyappan S, Arumugam R, Pichan K, Kasthuri R and Et. A 2017 Crystal growth and characterization of semi-organic 2-amino-5-nitropyridinium bromide (2A5NPBr) single

crystals for third-order nonlinear optical (NLO) applications Applied Physics A **12** 123. https://doi.org/10.1007/s00339-017-1394-3.

[31] Sakthy Priya S, Balakrishnan K, Surendran P, Lakshmanan A, Pushpalatha S, Rameshkumar P, Geetha P, Kannan K, Hegde T A and Vinitha G 2021 Investigation on nonlinear optical and antibacterial properties of organic single crystal: p-Toluidinium L-Tartrate Chemical Data Collections **31** 100640. https://doi.org/10.1016/j.cdc.2020.100640.

[32] Rajkumar R and Praveen Kumar P 2019 Structure, crystal growth and characterization of piperazinium bis(4-nitrobenzoate) dihydrate crystal for nonlinear optics and optical limiting applications Journal of Molecular Structure **1179** 108 -117. https://doi.org/10.1016/j.molstruc.2018.10.085.

[33] K. Jubi Initha Mary, A. Mohamad Asikali, and R. Rajesh Paulraj 2026 Tailoring piezoelectric and dielectric performance of TGS crystals through polyborate incorporation Appl. Phys. A **132** 346. https://doi.org/10.1007/s00339-026-09531-0.

[34] Wang Z, Lu L, Meng J and Wang T 2025 Emerging Negative Photoconductivity Effect-Based Synaptic Device for Optoelectronic In-Sensor Computing Advanced Materials **37** 2504710. https://doi.org/10.1002/adma.202504710.

[35] Sundareswaran T, Manikandan S, Rajesh P and Boaz B M 2025 Growth, elemental, spectral, linear, photoconductivity, dielectric, thermal, and Z-scan analysis of benzotriazolium oxalate dihydrate single crystal for third-order harmonic generation applications J Mater Sci: Mater Electron **36** 27. https://doi.org/10.1007/s10854-024-14053-7.

[36] Tamilarasi S, Sunwathi S P, Lasalle B S I, Sukumar K, Pandian M S, Janczak J and Kanagathara N 2026 Growth, optical, thermal, electrical and theoretical insights on bis (Glycinium) 1, 5- naphthalene disulfonate dihydrate (GNSH) single crystals for optical applications Materials Science and Engineering: B **326** 119219. https://doi.org/ 10.1016/j.mseb.2026.119219.

[37] Meenatchi V, Siva S and Cheng L 2021 Synthesis, crystal growth, spectroscopic characterization, Hirshfeld surface analysis and DFT investigations of novel nonlinear optically active 4-benzoylpyridine-derived hydrazone Journal of Molecular Structure **1243** 130858. https://doi.org/10.1016/j.molstruc.2021.130858.

[38] Vijayasri M, Archana N, Dayanidhi K, Dhanalakshmi M, Vinitha G and Parthiban S 2025 Crystal growth, structural insights, Hirshfeld surface analysis and nonlinear optical properties of bis (2-aminobenzothiazolium) hexachlorostannate (IV) **2**, Next Research 100707. https://doi.org/10.1016/j.nexres.2025.100707.

[39] Priya S S, Balakrishnan K, Lakshmanan A, Surendran P, Rameshkumar P, Kannan K, Geetha P, Hegde T A and Vinitha G 2020 Crystal growth and characterization of Benzimidazolium salicylate single crystal for nonlinear optical studies and antibacterial activity Physics and Chemistry of Solid State **21** 377–89. https://doi.org/10.15330/PCSS.21.3.377-389.

[40] S. Anbu Chudar Azhagan & V. Marianandhakumar Measurement of nonlinear refractive index, figure of merit, coupling factor of pure adipic acid crystals by Z-scan technique using continuous wave Nd:YAG laser | Journal of Materials Science: Materials in Electronics **36** https://doi.org/1034. 10.1007/s10854-025-15134-x.

[41] Sundareswaran T, Manikandan S, Rajesh P and Boaz B M 2025 Growth, elemental, spectral, linear, photoconductivity, dielectric, thermal, and Z-scan analysis of benzotriazolium oxalate dihydrate single crystal for third-order harmonic generation applications J Mater Sci: Mater Electron **36** 27. https://doi.org/10.1007/s10854-024-14053-7.

[42] Lasalle B S I, Pandian M S, Ramasamy P and Anitha K 2025 Synthesis, crystal growth, optical, thermal, electrical and theoretical investigation on 1,2,3- benzotriazole 2-chloro 4-nitrobenzoic acid (BCNB) single crystal for nonlinear optical (NLO) applications Inorganic chemistry communications 2023 **157** 111388. https://doi.org/10.1016/j.inoche.2023.111388.

[43] Chinnakannu E, Sankar M, Chandran S, Thamotharan K and Manickam S 2024 Crystal growth, structural, optical, computational, and Z-scan analyses of imidazolium hydrogen oxalate crystal for nonlinear optical applications Journal of Materials Research **39** 1246–57. https://doi.org/10.1557/s43578-024-01306-8.

[44] Blessy M L, Dhas D A, Joe I H and Vinitha G 2025 Crystal growth, spectroscopic investigation and z-scan analysis of novelly synthesized NLO active bis(2-amino-4,6-dimethoxypyrimidinium) 5-sulfosalicylate single crystal J Mater Sci: Mater Electron **36** 802. https://doi.org/10.1007/s10854-025-14765-4.

[45] Chinnakannu E, Sankar M, Chandran S, Thamotharan K and Manickam S 2024 Crystal Growth, Optical, Thermal, DFT and Z-Scan Studies of Imidazolium Hydrogen Fumarate Crystal for Nonlinear Optical Applications Crystal Research and Technology **59** 2300229. https://doi.org/10.1002/crat.202300229.

[46] Bhise V B and Dhokane G R 2025 A promising role of Ba^{2+} ion in the enhancement of structural, optical, photoluminescence, Z-scan, etching and laser damage threshold study of $C_6H_{14}N_4O_2H_3PO_4H_2O$ single crystals: Implications on photonics device applications Results in Optics **18** 100790. https://doi.org/10.1016/j.rio.2025.100790.



Figure 1: Photograph of grown PSA crystal

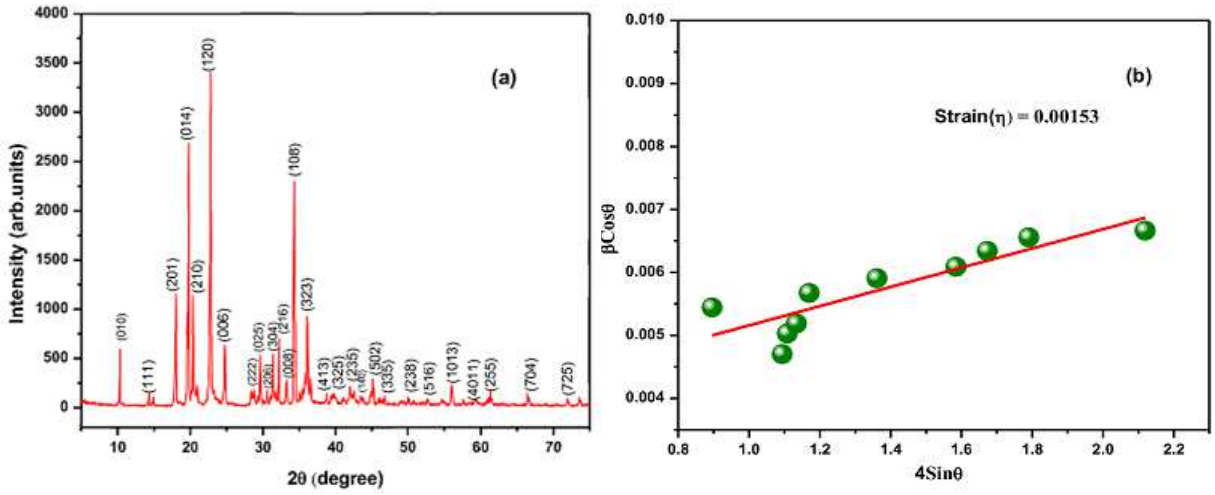


Figure 2: (a) X-ray diffraction pattern and (b) W -H plot of grown PSA crystal

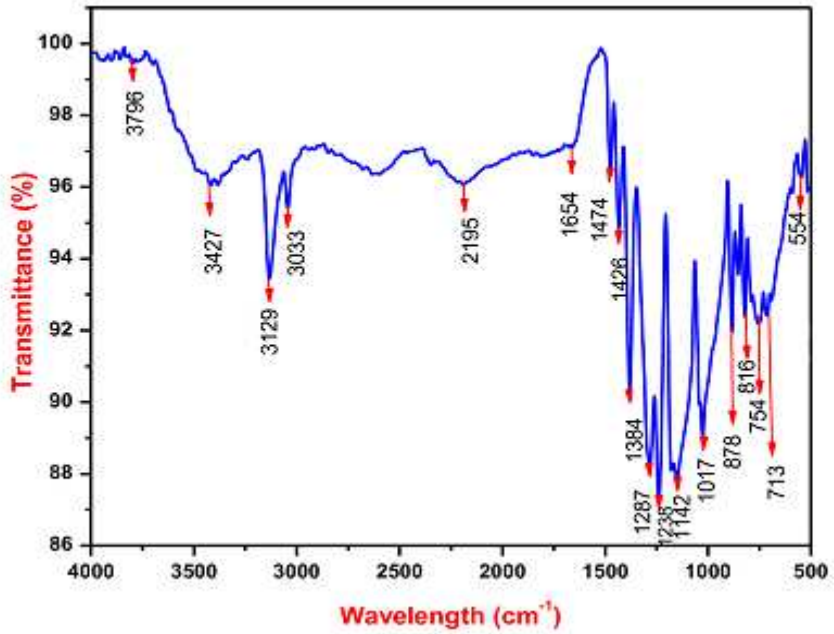


Figure 3: FTIR spectrum of PSA crystal

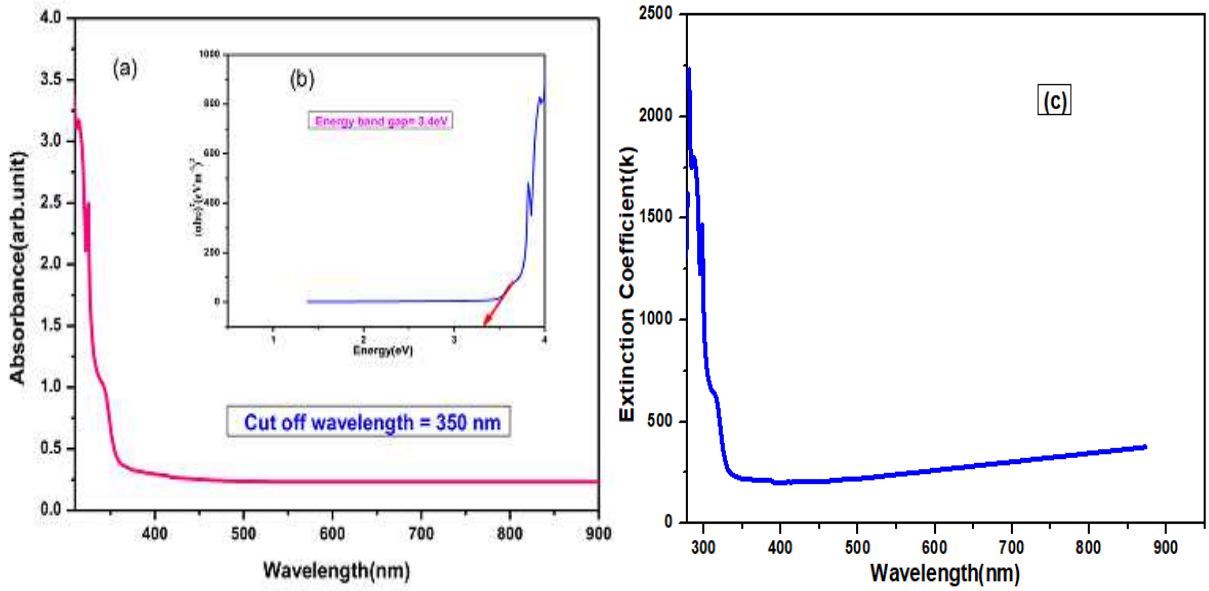


Figure 4: (a) UV-Visible absorption spectrum (b) Tauc's plot between $(\alpha h\upsilon)^2$ versus $h\upsilon$ and (c) Wavelength dependence of Extinction Coefficient (k) of the grown PSA crystal

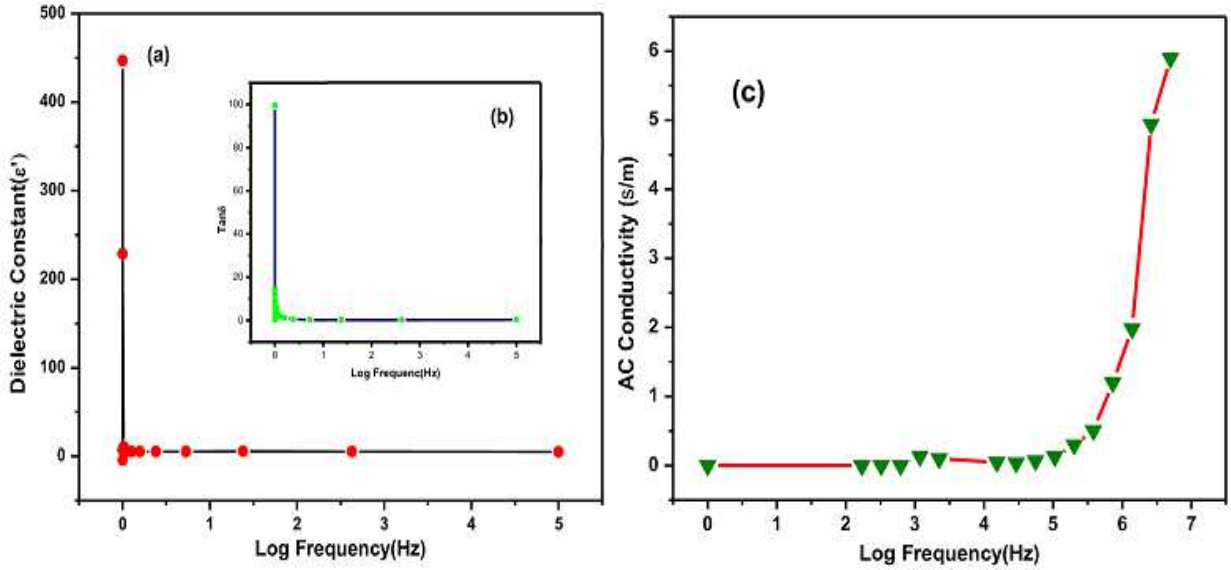


Figure 5 :(a) Plot of dielectric constant versus log frequency (b) Plot of dielectric loss Vs log frequency and (c) Plot of AC Conductivity versus log frequency of the grown PSA crystal

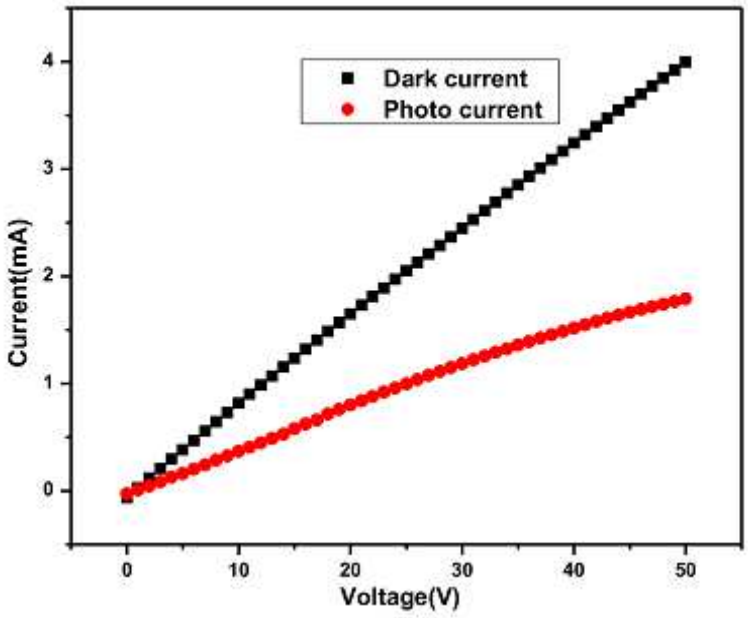


Figure 6: Photo Conductivity plot of the grown PSA crystal

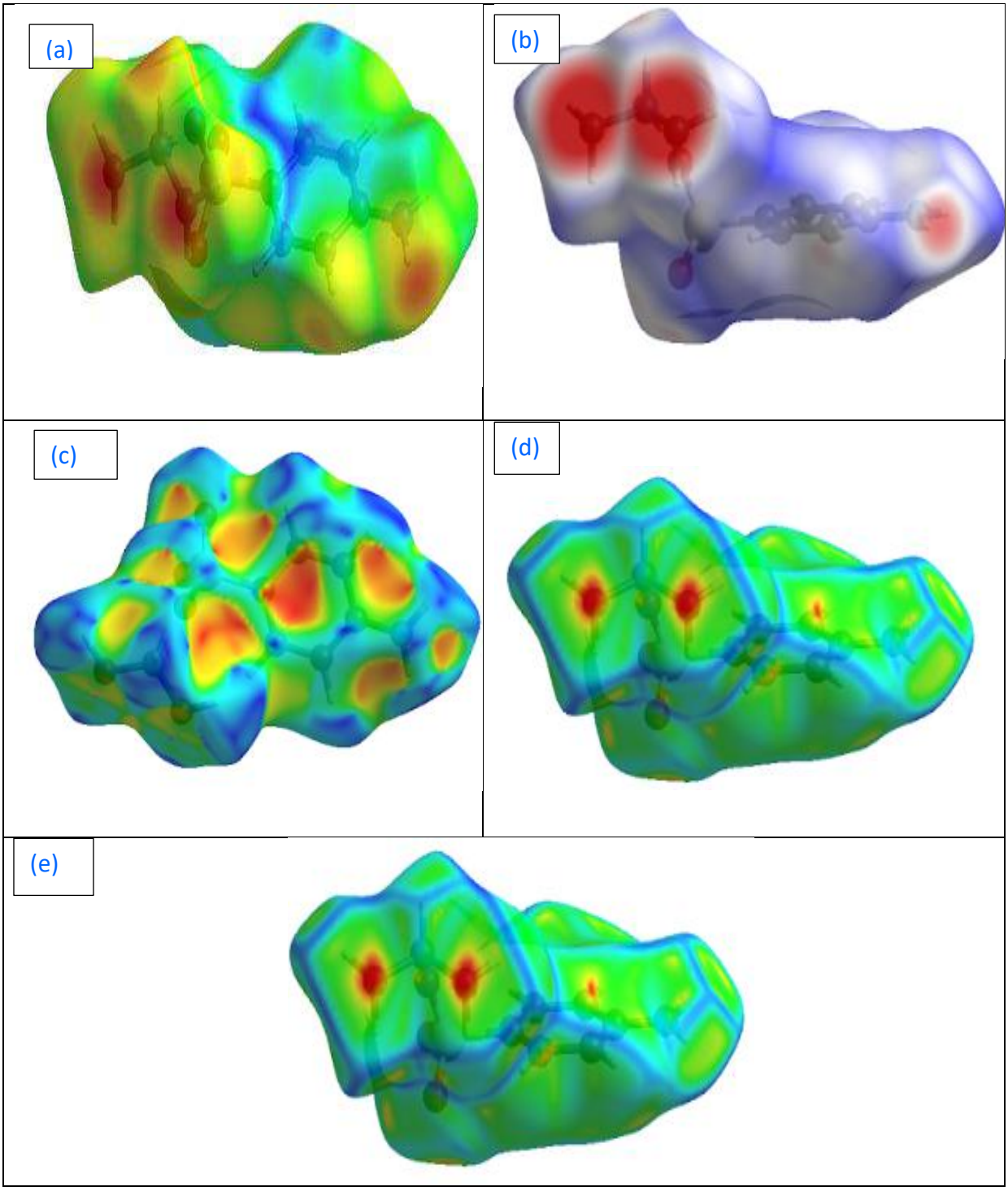
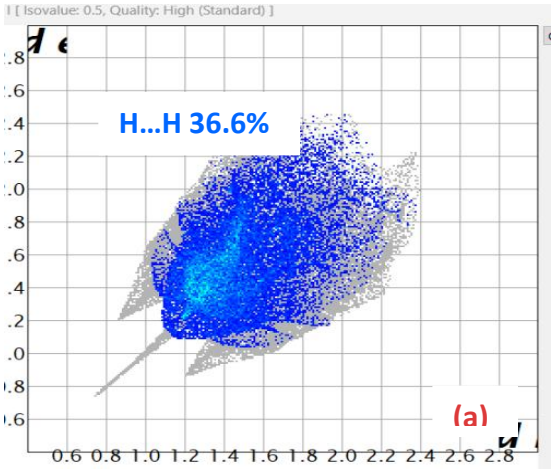
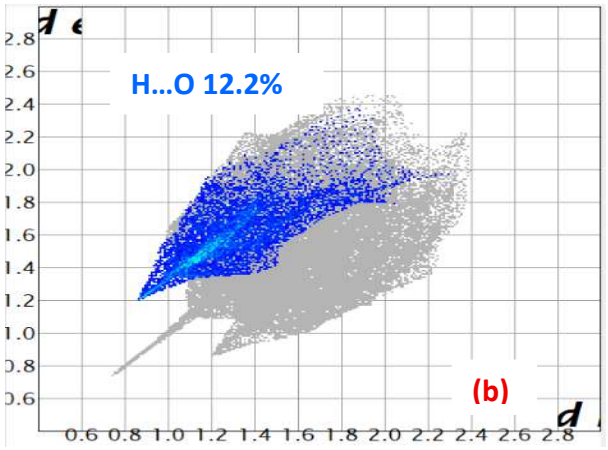
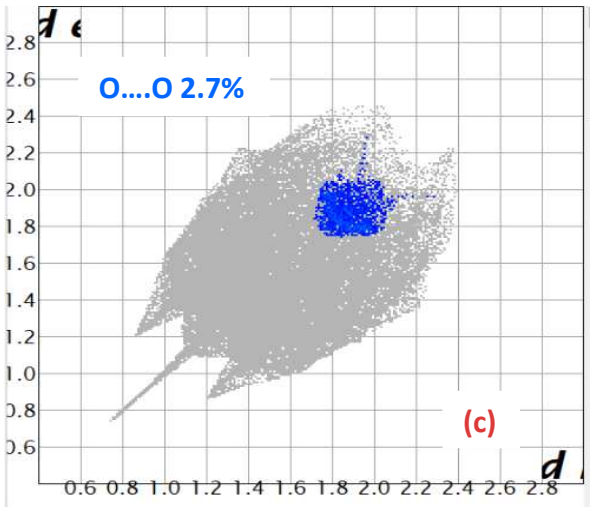
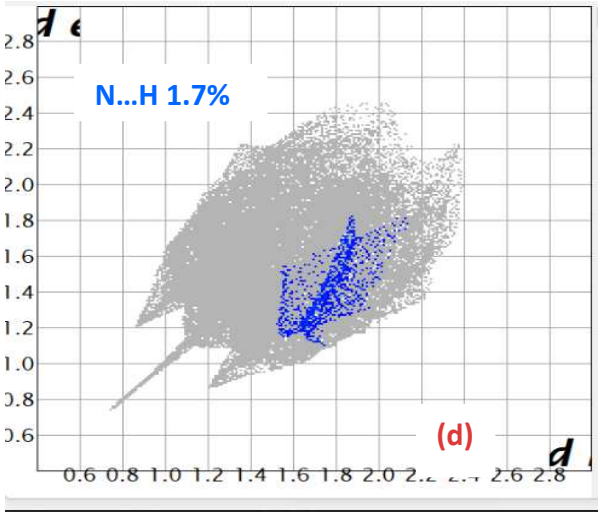


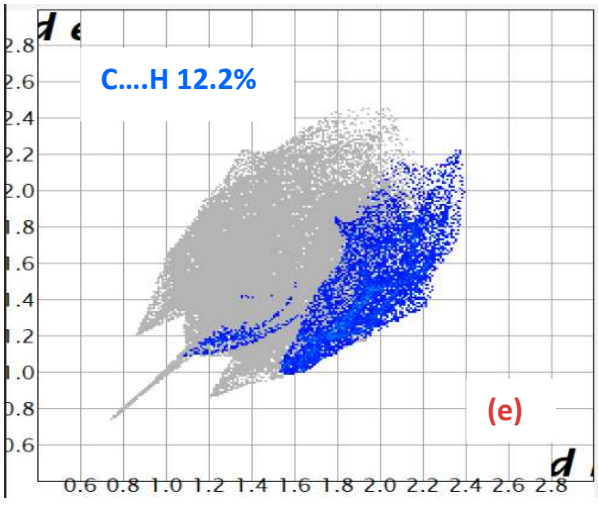
Figure 7: (a) di, (b) d_{norm} (c) Shape index, (d) Curvedness, and (e) Curvedness of Hirshfeld Surface PSA Crystal

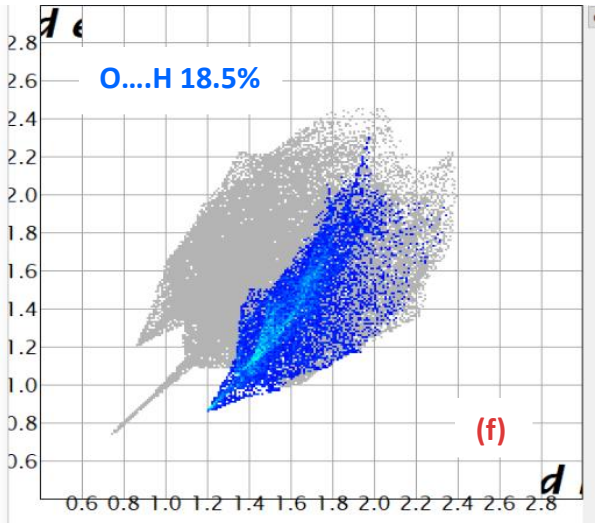

[Isovalue: 0.5, Quality: High (Standard)]
H...H 36.6%
(a)
0.6 0.8 1.0 1.2 1.4 1.6 1.8 2.0 2.2 2.4 2.6 2.8


H...O 12.2%
(b)
0.6 0.8 1.0 1.2 1.4 1.6 1.8 2.0 2.2 2.4 2.6 2.8


O....O 2.7%
(c)
0.6 0.8 1.0 1.2 1.4 1.6 1.8 2.0 2.2 2.4 2.6 2.8


N...H 1.7%
(d)
0.6 0.8 1.0 1.2 1.4 1.6 1.8 2.0 2.6 2.8


C....H 12.2%
(e)
0.6 0.8 1.0 1.2 1.4 1.6 1.8 2.0 2.2 2.4 2.6 2.8


O....H 18.5%
(f)
0.6 0.8 1.0 1.2 1.4 1.6 1.8 2.0 2.2 2.4 2.6 2.8

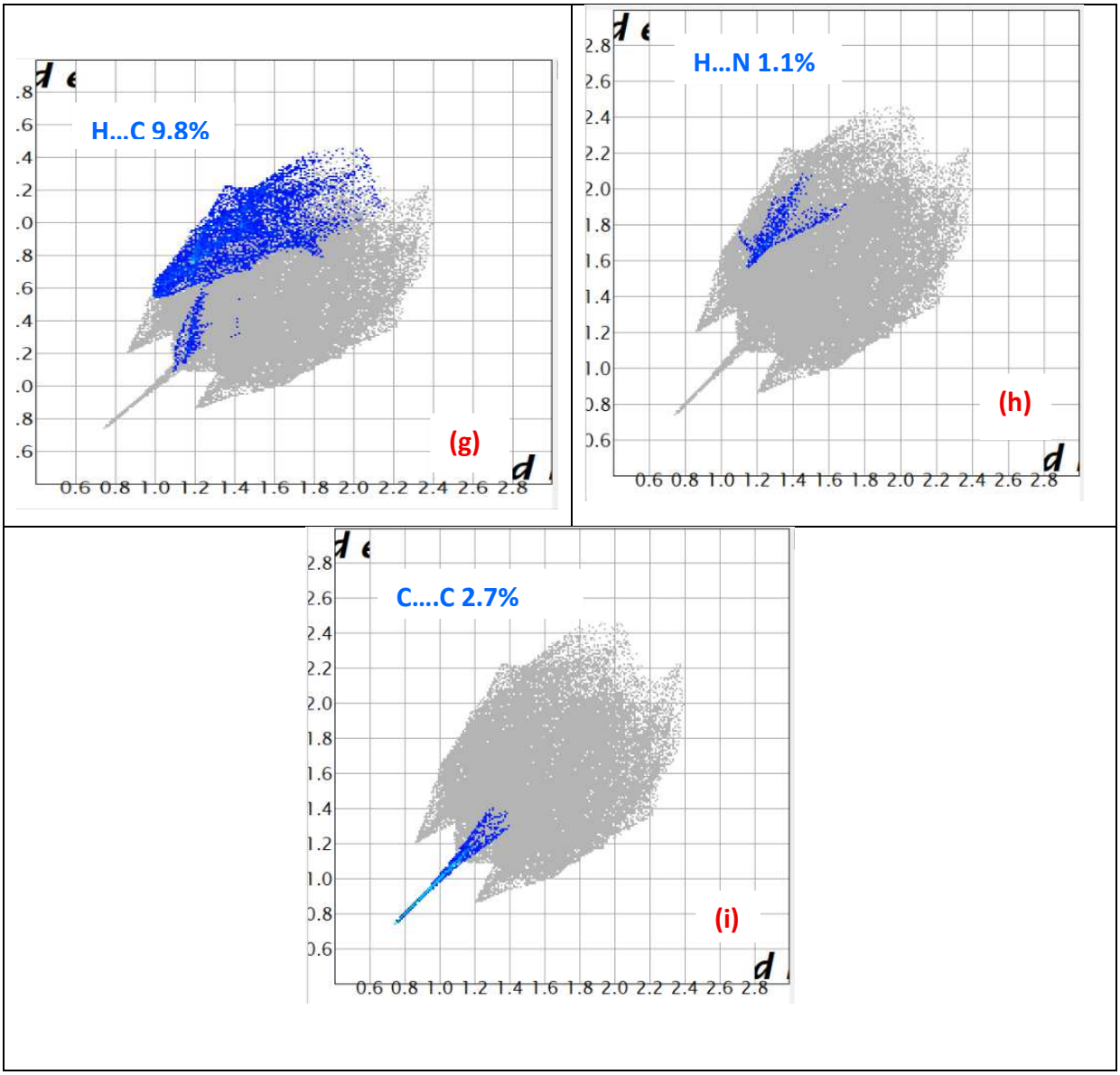


Figure 8: Two-dimensional fingerprint plots showing the contributions of atoms within specific interacting pairs (blue areas). For each fingerprint map, the gray area is a representation of the whole plot.

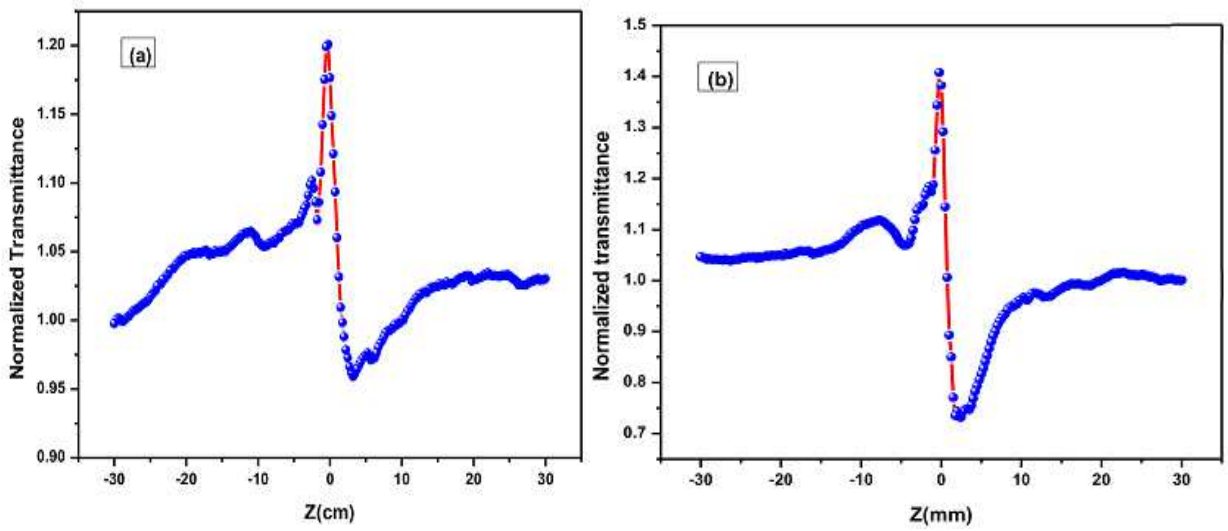


Figure 9: (a) Open aperture (b) closed aperture curve of PSA crystal

Table 1: Polarizability parameters of the grown PSA crystal

Parameters	**PSA(Present work)**	**2A5NPBr** [29]	**PTLT**[30]	**PNBA**[31]
Molecular weight(g/mol)	259.33	220.03	257.237	228.21
Density (g cm^{-3})	2.477714	1.887	1.3682	1.475
Plasma energy (eV)	24.8622	20.65	21.0039	18.9
Penn gap (eV)	1.699551732	1.344	1.9034	1.54
Fermi energy (eV)	21.1639	16.711	17.0668	14.8
Polarizability from Penn analysis (cm^3)	8.17×10^{-23}	4.55×10^{-23}	7.26×10^{-23}	6.003×10^{-23}
Polarizability from Clausius-Mossotti equation (cm^3)	8.19×10^{-23}	4.57×10^{-23}	7.28×10^{-23}	6.015×10^{-23}

Table 2: Percentage contribution of interaction of atom of Hirshfield surface analysis

Intermolecular Contacts	Percentage
H…H	36.2
C…H	12.2
O…O	2.7
H…O	14.7
N…H	1.7
O…H	18.5
H…N	1.1
H…C	9.8
C…C	2.7

Table 3: Third order (NLO) parameters of the grown PSA crystal

Parameters	Values
Laser wavelength	632.8(nm)
Focal length of lens used	300(mm)
Intensity of laser at the focus	30.6(MW/m^2)
Nonlinear refractive index ($n_{2)}$	1.94125 x 10^{-9}(cm^2/W)
Linear absorption coefficient (β)	8.47049 x 10^{-4}(cm/W)
Real Part of third-order NLO susceptibility ($Re\chi^{(3)}$)	7.45303 x 10^{-8} (esu)
Imaginary part of third- order NLO susceptibility ($Im\chi^{(3)}$)	1.6385 x 10^{-6}(esu)
Third-order nonlinear Susceptibility ($\chi^{(3)}$)	7.630976 x 10^{-7}(esu)

Table 4: Comparison of third order nonlinear optical susceptibility $\chi^{(3)}$ values of PSA with other NLO materials

Crystal	Third order NLO susceptibility $\chi^{(3)}$	Reference
PSA	7.630976 x 10^{-7}(esu)	Present work
BCNB	2.38179×10^{-8} esu	[42]
IHO	2.6422 × 10^{-9} esu.	[43]
B2AD5SSA	6.58 x 10^{-6} esu	[44]
IHF	2.08934 × 10^{-9} esu.	[45]
Ba-Lap	7.2169 × 10^{-10} esu	[46]